

# M87 as a misaligned Synchrotron-Proton Blazar

A. Reimer<sup>1</sup>, R.J. Protheroe<sup>2</sup>, and A.-C. Donea<sup>2</sup>

<sup>1</sup> Institut für Theoretische Physik, Lehrstuhl IV: Weltraum- & Astrophysik, Ruhr-Universität Bochum, D-44780 Bochum, Germany  
e-mail: afm@tp4.rub.de

<sup>2</sup> Department of Physics and Mathematical Physics, The University of Adelaide, Adelaide, SA 5005, Australia  
e-mail: rprother@physics.adelaide.edu.au, adonea@physics.adelaide.edu.au

Received August 27, 2003; accepted February 3, 2004

**Abstract.** The giant radio galaxy M87 is usually classified as a Fanaroff-Riley class I source, suggesting that M87 is a mis-aligned BL Lac object. Its unresolved nuclear region emits strong non-thermal emission from radio to X-rays which has been interpreted as synchrotron radiation. In an earlier paper we predicted M87 as a source of detectable gamma ray emission in the context of the hadronic Synchrotron-Proton Blazar (SPB) model. The subsequent tentative detection of TeV energy photons by the HEGRA-telescope array would, if confirmed, make it the first radio galaxy to be detected at TeV-energies. We discuss the emission from the unresolved nuclear region of M87 in the context of the SPB model, and give examples of possible model representations of its non-simultaneous spectral energy distribution. The low-energy component can be explained as synchrotron radiation by a primary relativistic electron population that is injected together with energetic protons into a highly magnetized emission region. We find that the  $\gamma$ -ray power output is dominated either by  $\mu^\pm/\pi^\pm$  synchrotron or proton synchrotron radiation depending on whether the primary electron synchrotron component peaks at low or high energies, respectively. The predicted  $\gamma$ -ray luminosity peaks at  $\sim 100$  GeV at a level comparable to that of the low-energy hump, and this makes M87 a promising candidate source for the newly-commissioned high-sensitivity low-threshold Cherenkov telescopes H.E.S.S., VERITAS, MAGIC and CANGAROO III. Because of its proximity, the high-energy spectrum of M87 is unaffected by absorption in the cosmic infrared (IR) background radiation field, and could therefore serve as a template spectrum for the corresponding class of blazar if corrected for mis-alignment effects. This could significantly push efforts to constrain the cosmic IR radiation field through observation of more distant TeV-blazars, and could have a strong impact on blazar emission models. If M87 is a mis-aligned BL-Lac object and produces TeV-photons as recently detected by the HEGRA-array, in the context of the SPB model it must also be an efficient proton accelerator.

**Key words.** Galaxies: active – Galaxies: individual: M87 – Gamma rays: theory – Radiation mechanisms: non-thermal

## 1. Introduction

The Fanaroff-Riley (FR) class I giant radio galaxy M87, situated nearly at the center of the Virgo cluster, was the first extragalactic jet to be discovered (Curtis (1918)), and has since then been intensively observed at all wavelengths. Its proximity ( $\sim 16.3$  Mpc; Cohen et al. (2000)) makes it an interesting laboratory for testing and understanding extragalactic jets of radio-loud Active Galactic Nuclei (AGN) and their powering engines.

Because M87 is sufficiently near for ultra-high-energy cosmic rays (UHECRs) to be little affected by the GZK-cutoff at  $\sim 5 \times 10^{19}$  eV (Greisen (1966), Zatsepin & Kuz'min (1966)), and because its size scales could allow magnetic confinement of the most energetic cosmic rays (Hillas (1984)), M87 has long been considered as one of the prime candidate sources of high energy cosmic rays. This idea has recently received some support by the suggestion that possible clustering observed in the arrival directions of the UHECRs can be understood in terms of deflection of UHECRs from M87 by our Galaxy's magnetized wind assuming a Parker-spiral magnetic structure (Ahn et al. (1999); Biermann et al. (2001)). It appears, however, that such deflection in the Galactic wind may be insensitive to the direction of the cosmic ray sources (Billoir & Letessier-Selvon (2000)). Nevertheless, Protheroe et al. (2003) found by using the cosmic ray output predicted in the SPB model that M87 could explain the observed UHECR flux if

the magnetic field topology between M87 and our Galaxy were favourable. They found that UHECR with energies above  $10^{20}$  eV could easily be produced because neutrons produced in the pion photoproduction process would be relativistically beamed along the jet direction and Doppler boosted in energy. Even though M87's jet is mis-aligned with respect to our line-of-sight, these Doppler boosted neutrons escape from the jet and decay into UHECRs which maintain their Doppler boosted energies and may propagate in all directions, including towards our Galaxy if the magnetic field topology were favourable. Of course we note that M87's nuclear region is not the only possible source of the UHECRs observed at Earth; see e.g. Protheroe & Clay (2004) for a recent review.

According to the unification model of AGN (e.g. Urry & Padovani (1995)) FR I radio galaxies, with their jet axis at a large angle to our line-of-sight, are the parent population of BL Lac objects whose jets are closely aligned to our line-of-sight. This motivates us to consider M87's nuclear region as a mis-aligned blazar of BL Lac type. The spectral energy distribution (SED) of BL Lac objects can usually be explained satisfactorily by either leptonic or hadronic blazar emission models. Bai & Lee (2001) have discussed M87 on the basis of the leptonic Synchrotron-Self Compton (SSC) model where synchrotron photons produced by interactions of relativistic electrons with the ambient magnetic field serve as the target photons for inverse Compton scattering by the same electrons. By interpreting the non-thermal radiation from the radio to the X-ray band as synchrotron emission with luminosity peaking in the far-ultraviolet, the authors considered M87 to be a mis-aligned high-frequency peaked BL Lac (HBL), and predicted  $\gamma$ -ray emission with an inverse Compton peak at  $\sim 100$  GeV. The predicted inverse Compton flux is consistent with the recent HEGRA detection of M87 (Aharonian et al. (2003), see Sect. 2). Detectable TeV-emission from Comptonization of galactic photon fields has recently been suggested by Stawarz et al. (2003). In contrast to former models, they consider, however, the large scale jet to be the site of  $\gamma$ -ray production.

While in leptonic models a relativistic electron-positron plasma is usually assumed to be responsible for the non-thermal jet radiation, in hadronic models a relativistic proton-electron ( $p e^-$ ) plasma is assumed to be the main constituent of the jet material. In the hadronic Synchrotron-Proton Blazar (SPB) model, proposed recently by, e.g., Mücke & Protheroe (2001), accelerated protons interact with the synchrotron radiation field produced by the co-accelerated electrons via meson photoproduction and Bethe-Heitler pair production and, more importantly, with the strong ambient magnetic field emitting synchrotron radiation (mesons and muons also emit synchrotron radiation). The SPB model neglects external photon field components, and this seems appropriate for BL Lac objects and their parent population which possess only weak accretion disks. Mücke & Protheroe (2001) have shown that this model can reproduce the commonly observed double-humped blazar SED. Hadronic models require high proton energies that can only be achieved in a highly magnetized environment where synchrotron losses can become severe. Magnetic field values around  $10^3$  G are thought to exist near the horizon of a supermassive black hole (Blandford & Znajek (1977)) with a mass of  $\sim 10^9 M_\odot$  as estimated for M87 (Marconi et al. (1997)). However, with M87's rather low accretion rate if the equipartition value of  $B$  scales with  $\dot{M}$ , and assuming magnetic energy flux conservation, magnetic field strengths of order 10-100 Gauss are expected within 30 Schwarzschild radii  $r_g$  where the jet is probably formed (Junor & Biretta (1999)). In the present work, we discuss in more detail than our earlier work (Protheroe et al. (2003)), and in the context of the recent HEGRA detection (Aharonian et al. (2003)), the nuclear (core) emission, i.e. from the M87 jet, in the framework of the SPB-model.

In Section 2 we summarize the data on M87's core emission. In section 3 we give a brief model description, and calculate the steady-state synchrotron component as described in the appendix. The modeling procedure is described in section 4, and we conclude with a summary and discussions in section 5.

## 2. The data

Speculation that M87 could be a powerful accelerator of cosmic rays triggered space-based  $\gamma$ -ray detectors and ground-based high-sensitivity Cherenkov telescopes to search for  $\gamma$ -ray emission from this radio galaxy. Until recently, only upper limits were obtained. From EGRET data Reimer et al. (2003) obtained  $F(>100 \text{ MeV}) < 2.2 \times 10^{-8} \text{ cm}^{-2} \text{ s}^{-1}$ . Using Whipple data from 2000-2001 (Le Bohec et al. (2001)) and 2002-2003, Le Bohec et al. (2003) obtained  $F(>250 \text{ GeV}) < 2.6 \times 10^{-11} \text{ cm}^{-2} \text{ s}^{-1}$ . Using 1998-1999 data from HEGRA telescope array Götting et al. (2001) obtained  $F(> 720 \text{ GeV}) < 1.45 \times 10^{-12} \text{ cm}^{-2} \text{ s}^{-1}$  (at the  $3\sigma$  level). By doubling the data set and applying a more sensitive analysis method, the HEGRA team has recently been published the first (though tentative) detection of  $> 730$  GeV photons at the  $4\sigma$  level (Aharonian et al. (2003)). This detection, which does not contradict the Whipple upper limits, places the first data point in the so-far rather unconstrained high energy regime of M87's SED, and has motivated us to refine our previous modeling attempt and predictions for  $\gamma$ -rays from this source (Protheroe et al. (2003)).

The non-simultaneous SED is shown in Fig. 1 and 3. The data imply that the synchrotron spectrum from the primary electrons must exhibit a break frequency at either a few  $10^{12}$ Hz (Perlman et al. (2001)) or around  $10^{14}$ Hz. Break frequencies above  $10^{14}$ Hz as proposed by Bai & Lee (2001) seem unreasonable to us given the fact that, firstly, the EUVE data point from Berghöfer et al. (2000) with its considerably lower resolution compared to the other data points should effectively be considered rather as an upper limit, and secondly, the recent flux measurements from the

Chandra observatory (Wilson & Yang (2002)) point to a much steeper spectrum in the X-ray band than anticipated by Bai & Lee (2001). Note, however, that variability effects may play a crucial role here. Another interesting spectral feature is the strong steepening by  $\Delta\alpha \approx 1$  that occurs around IR/optical wavelengths, which can not easily be explained by a transition from escape dominated to synchrotron cooling dominated electron energy losses.

Images from the VLA (Biretta et al. (1995)), HST (Sparks et al. (1996), Biretta et al. (1999)), Gemini (Perlman et al. (2001)) and Chandra (Wilson & Yang (2002), Harris et al. (2003)) of the so-far unresolved core of M87 are at present at the sub-arcsec scale, giving a metric resolution of order 1-10 pc. Sub-mas scale cm and mm wavelength intercontinental VLBI (Junor & Biretta (1995), Junor & Biretta (1999)) provide the highest linear resolution of  $\sim 0.01$  pc achieved on any extragalactic radio jet so far, and thereby place the most stringent upper limit on the size of the radio emitting region. Striking variability in the core region has not only been observed in the radio to optical band, but has also been deduced from Chandra X-ray monitoring in 2002 (Harris et al. (2003)). An observed flux increase of about 20% which has been measured within 46 days can be transformed into a doubling time of about 77 days, and provides a limit for the source size of the X-ray emitting region of  $R \simeq 0.1$ pc.

HST data (Biretta et al. (1999)) show that features within the first arcsec of the jet move only at sub-luminal speeds, while at larger distances from the core super-luminal motion is observed. In this work we assume that the pattern speed equals the flow velocity of the knots, or “plasmoids”. The upstream knot closest to the core has an apparent speed of  $0.63 \pm 0.23c$  which we use here to constrain the beaming factor for the nuclear emission. For a jet angle between  $10^\circ - 40^\circ$  as suggested from VLA and HST proper motion studies (Biretta et al. (1995), Biretta et al. (1999)) we find that Doppler factors in the range  $D = 1.5 - 3$  are consistent with the apparent bulk speed.

### 3. The model

We assume the emission region, or “blob”, in an AGN jet moves relativistically with Lorentz factor  $\Gamma_j$  and velocity  $\beta_j c$  along the jet axis. We further assume that relativistic (accelerated) protons, whose particle density  $N'_p$  follows a power-law spectrum  $\propto \gamma_p'^{-\alpha_p}$  in the range  $2 \leq \gamma_p' \leq \gamma_{p,\max}'$  (primed quantities are in the jet frame), are injected instantaneously into a highly magnetized environment ( $B'$  is constant within the emission region), and that they remain quasi-isotropic in the jet frame due to pitch-angle scattering. The proton energy-loss processes considered in the model are photomeson production, Bethe-Heitler pair production, proton synchrotron radiation and adiabatic losses due to jet expansion. Synchrotron radiation prior to their decay from  $\pi^\pm$  (from photomeson production) and  $\mu^\pm$  (from  $\pi^\pm$  decay) becomes important in highly magnetized environments (Rachen & Mészáros (1998)), and is taken into account in our calculations. We assume that the maximum particle energies are limited by the balance between energy gain and loss rates. The acceleration rate for any acceleration mechanism is  $dE'/dt' = \xi(E')ZecB'$  where  $\xi(E') \leq 1$  is the acceleration rate factor and  $Ze$  is the charge. If particles gain energy by diffusive shock acceleration and the spectra of both electrons and protons are cut off by synchrotron losses at Lorentz factors  $\gamma_{e,\max}$  and  $\gamma_{p,\max}$ , respectively, then

$$\frac{\xi(E_{e,\max})}{\xi(E_{p,\max})} = \left(\frac{m_e}{m_p}\right)^{4(1-\delta)/(1+\delta)} \quad (1)$$

if the diffusion coefficient has energy dependence  $\kappa(E) \propto E^\delta$  (see Appendix A). Thus for a Kolmogorov spectrum of turbulence, for which  $\delta=1/3$ ,  $\xi(E_{e,\max})/\xi(E_{p,\max}) = (m_e/m_p)^2 \approx 3 \times 10^{-7}$ .

The relativistic primary  $e^-$ , injected into the emission region with a power law particle distribution  $\propto E^{-\alpha_e}$ , radiate synchrotron photons that manifest themselves in the blazar SED as the synchrotron hump, and serve as the target radiation field for proton-photon interactions, and for the subsequent pair-synchrotron cascade which develops as a result of photon-photon pair production in the magnetized blob. The steady-state primary electron spectrum in the co-moving frame of the emission region is calculated as in Appendix A taking into account synchrotron and escape losses. The resulting synchrotron radiation from this particle distribution is then corrected for synchrotron-self absorption. For  $B' > 0.6(u'_{\text{phot}}/10^{10}\text{eV cm}^{-3})^{1/2}$  Gauss the target photon density  $u'_{\text{phot}}$  is smaller than the magnetic field energy density. Thus Inverse Compton losses can in most cases be neglected in the SPB model, and the corresponding SSC component is expected to be low compared to the primary synchrotron ‘hump’. However, for completeness we have calculated explicitly the SSC radiation from the primary electron component (see Appendix A).

The pair-synchrotron cascade redistributes the photon power to lower energies where the photons eventually escape from the emission region of size  $R'$ . The cascades can be initiated by photons from  $\pi^0$ -decay (“ $\pi^0$  cascade”), electrons from the  $\pi^\pm \rightarrow \mu^\pm \rightarrow e^\pm$  decay (“ $\pi^\pm$  cascade”),  $p$ -synchrotron photons (“ $p$ -synchrotron cascade”), charged  $\mu^-$ ,  $\pi^-$  and  $K$ -synchrotron photons (“ $\mu^\pm$ -synchrotron cascade”) and  $e^\pm$  from the proton-photon Bethe-Heitler pair production (“Bethe-Heitler cascade”). Direct proton and muon synchrotron radiation is mainly responsible for the high energy hump whereas the low energy hump is dominated by synchrotron radiation from the primary  $e^-$ , with a contribution of synchrotron radiation from secondary electrons produced by the  $p$ -synchrotron and  $\mu^\pm$ -synchrotron cascades. The

contribution from Bethe-Heitler pair production turned out to be negligible. For our calculations we use a Monte-Carlo method and utilize the recently developed SOPHIA code for the photohadronic event generation (Mücke et al. (2000)). In practice, to save CPU-time the target photon field is parametrized as a multiple broken power-law, which is then used as an input into the SOPHIA code.

## 4. Modeling the SED of M87

From variability and direct imaging arguments an upper limit for the size of M87’s emission region of a few  $10^{16}$ cm in the observer frame can be deduced. Together with the constraints from proper motion measurements, a reasonable parameter space for the modeling procedure is  $R' = 10^{15...16}$ cm and bulk Doppler factors  $D = 1.5 \dots 3$ . Furthermore we demand approximate equipartition between magnetic  $u'_B$  and particle energy density ( $u'_p + u'_e \approx u'_p$ ). This in general minimizes the total jet power for a given parameter set (Mücke & Protheroe (2001)). The observed synchrotron hump in the SED implies a break in the primary electron spectrum. A peak in the “synchrotron hump” in the SED is expected at either mm-wavelengths or in the optical. In the following we shall model both possibilities in turn, i.e. a high and low energy peak.

### 4.1. High-energy peaked synchrotron component (Model H)

The HEGRA-detection at sub-TeV energies places an important constraint on the models: protons must be accelerated to energies above  $10^{10}$ GeV. This can only be achieved by high magnetic field values, and/or a thin target photon field to prevent excessive losses at the highest energies. Typical magnetic field values in the SPB-model lie around several 10 G. Fig. 1 shows a reasonable representation of the data where we have used  $B' = 30$  G ( $u'_B = 2 \times 10^{13}$  eV cm $^{-3}$ ) and the primary synchrotron component peaking at about 1 eV. With a Doppler factor of  $D = 2$  and an observer-frame size of the emission region of  $R \approx 10^{15}$  cm the target photon density is  $u'_{\text{phot}} \approx 3 \times 10^{10}$  eV cm $^{-3}$ , and so the SSC component is negligible in Model H. Proton synchrotron losses dominate at the highest proton energies for this parameter set (see Fig. 2), and determine the cutoff energy and the  $\gamma$ -ray output from  $\sim 1$  TeV down to  $\sim 10$  MeV. At 0.1-10 MeV synchrotron radiation from a secondary  $e^\pm$  population produced by the reprocessed  $\mu^\pm/\pi^\pm$  synchrotron radiation dominates and produces a broad “valley” in the SED between the low and high energy humps that possess approximately equal power. An acceleration rate factor at the maximum proton energy  $\xi(E'_{p,\text{max}}) \approx 1$  is necessary to allow the injection proton spectrum to extend up to  $\gamma'_{p,\text{max}} = 3 \times 10^{10}$ .

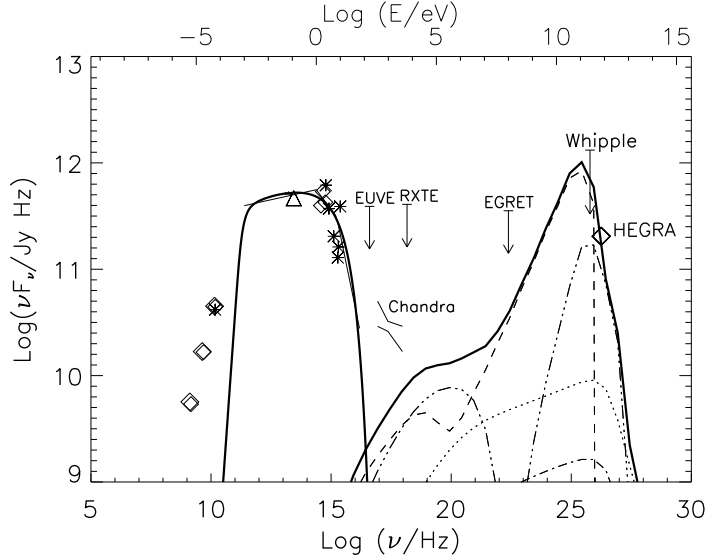
The primary electron synchrotron spectrum shows a low-energy break at the synchrotron self-absorption turnover energy of  $\sim$  a few  $10^{-4}$  eV, followed by a nearly flat power distribution, and then a turnover at about a few eV with a subsequent steep tail due to the cutoff in the electron distribution. Note that interpreting the strong steepening at a few eV in the data (see Sect. 2) as being due to a cutoff in the electron spectrum allows spectral breaks larger than 0.5. The high magnetic field leads to a dominance of synchrotron losses throughout the emitted low-energy component (the escape loss dominated energy range lies below the synchrotron-self absorption turnover frequency).

The total jet power for this parameter choice is  $L_{\text{jet}} \approx 3 \times 10^{43}$ erg/s, about the value for the jet kinetic power derived by Reynolds et al. (1996), but still below the nuclear power of M87 for accretion at the Bondi spherical rate ( $\sim 5 \times 10^{44}$  erg/s, Di Matteo et al. (2003)). The small radiative efficiency of the accretion disk and the fact that the radio power of M87 is low provides a natural explanation that M87 is a FRI source. Owen et al. (2000) have calculated the total bolometric luminosity of the order of  $10^{42}$  erg/s, in agreement with the total radiative output in the present models, which suggests that the jet in M87 is also a low efficiency radiator and that M87 is currently in a dormant activity stage.

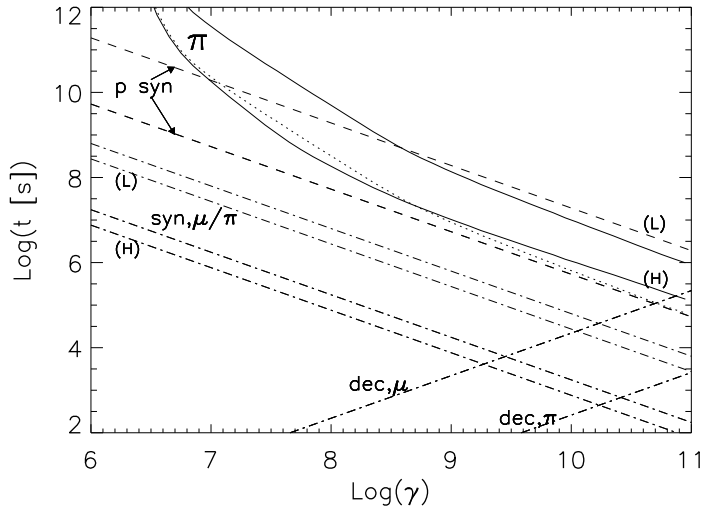
### 4.2. Low-energy peaked synchrotron component (Model L)

Fig. 3 shows an example for a model in which the primary electron synchrotron component peaks at  $\sim 10^{-3}$ eV. Here we have chosen the size of the emission region to be of the order of the limiting size from direct VLBI imaging, i.e.  $\sim 0.01$  pc (see Sect. 2). With  $D = 1.5$  and  $R \approx 10^{16}$  cm the jet-frame target photon density is low,  $u'_{\text{phot}} \approx 2 \times 10^9$  eV cm $^{-3}$ . A relatively low magnetic field strength of  $B' = 5$  G gives equipartition between magnetic and particle energy densities.

Despite the lower target photon energy density (down by a factor  $\sim 10$  compared to model H) pion photoproduction losses dominate at the highest energies for this parameter set (see Fig. 2) since the magnetic energy density is reduced by even more (down by a factor 36 compared to model H). In fact, even for models with identical magnetic and target photon energy densities, a lower break-energy in the target spectrum would cause a turnover in the  $\pi$  production losses at correspondingly higher proton energies and this would in turn result in a significantly higher  $\pi$  production loss rate at the highest proton energies. This is demonstrated in Fig. 2 where we compare the  $\pi$  production loss rate



**Fig. 1.** Non-simultaneous SED of M87's core compared with Model H fit. Data are from; Biretta et al. (1991) (diamonds); HST –Sparks et al. (1996) (stars); Gemini – Perlman et al. (2001) (triangle); EUVE – Berghöfer et al. (2000) (assuming a ratio for the jet/core flux of 1.5), RXTE – Reynolds et al. (1999); Chandra – Wilson & Yang (2002); EGRET –Reimer et al. (2003); Whipple – Le Bohec et al. (2001); HEGRA – Götting et al. (2001) and Aharonian et al. (2003). Flux uncertainties range from  $\sim 20\%$  (radio-to-optical data) to  $26\%$  (HEGRA data point). The uncertainty of the Chandra measurements is indicated. Flux variability may add to these uncertainties. Model H parameters are:  $B' = 30$  G,  $D = 2$ ,  $R' \approx 2 \times 10^{15}$  cm,  $u'_{\text{phot}} \approx 3 \times 10^{10}$  eV  $\text{cm}^{-3}$ ,  $u'_p = 15$  erg  $\text{cm}^{-3}$ ,  $e/p \approx 7.6$ ,  $\alpha_e = \alpha_p = 1.9$ ,  $L_{\text{jet}} \approx 2.5 \times 10^{43}$  erg/s,  $\gamma'_{p,\text{max}} = 3 \times 10^{10}$ ,  $\xi(E'_{p,\text{max}}) \approx 1$ ,  $\xi(E'_{e,\text{max}}) = 7 \cdot 10^{-8}$ . The target photon field for  $p - \gamma$  interactions is the primary electron synchrotron photon field, approximated by broken power laws (thin solid line) with break energies  $\epsilon_{b,1} = 1$  eV and  $\epsilon_{b,2} = 7$  eV between  $8 \cdot 10^{-4}$  eV and 70 eV in the observer frame and photon spectral indices  $\alpha_1 = 1.95$ ,  $\alpha_2 = 2.3$  and  $\alpha_3 = 3.1$ . The total cascade spectrum (solid line) is the sum of  $p$  synchrotron cascade (dashed line),  $\mu$  synchrotron cascade (dashed-triple dot),  $\pi^0$  cascade (dotted line) and  $\pi^\pm$ -cascade (dashed-dotted line). The expected SSC component covers the X-ray regime with a flux level that is not visible in this figure.



**Fig. 2.** Mean energy loss times (jet frame) for Models (H) and (L) for  $\pi$ -photoproduction ( $\pi$ , solid lines) and proton synchrotron radiation (p syn, dashed line). While in model (H) p synchrotron losses dominate, in model (L)  $\pi$  production losses become dominant at the highest proton energies. Loss times for  $\pi^\pm$  and  $\mu^\pm$  synchrotron radiation (syn  $\pi$ , syn  $\mu$ ) are also shown and compared with their mean decay time scales (dec  $\pi$ , dec  $\mu$ ). The dotted line represents the  $\pi$  production loss time scale for the same target photon density as used in model (H) but with a spectral distribution as in model (L). Lowering the target field's peak energy leads to an increase of the  $\pi$  production rate at the highest proton energies.

of the present parameter set (Model L) with the corresponding rate for the same target spectrum but normalized up to the photon energy density as used in Model H. We conclude that in radiation fields that peak at high energies  $p$ -synchrotron losses dominate, while in low-energy-peaked target photon fields  $\pi$  production losses dominate at the highest proton energies for equal magnetic and target photon energy densities.

For modeling the primary synchrotron spectrum peaking at around  $10^{-3}$  eV we have injected a softer electron distribution ( $\alpha_e = 2.1$ ) into the emission region. The turnover at this energy is due to synchrotron-self absorption

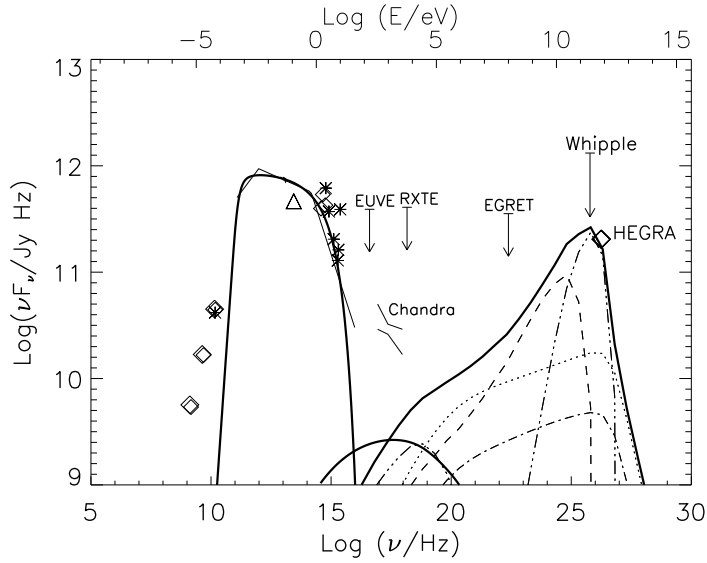


**Fig. 3.** Model L. Parameters are:  $B' = 5$  G,  $D = 1.5$ ,  $R' = 2 \times 10^{16}$  cm,  $u'_{\text{phot}} = 2 \times 10^9$  eV cm $^{-3}$ ,  $u'_p \approx 1$  erg cm $^{-3}$ ,  $e/p \approx 7$ ,  $\alpha_e = \alpha_p = 2.1$ ,  $L_{\text{jet}} \approx 9 \times 10^{43}$  erg/s,  $\gamma'_{p,\text{max}} = 4 \times 10^{10}$ ,  $\xi(E'_{p,\text{max}}) \approx 1$ ,  $\xi(E'_{e,\text{max}}) = 3 \cdot 10^{-8}$ . For the the target photon field (thin solid line) we used  $\alpha_1 = 1.7$ ,  $\alpha_2 = 2.1$ ,  $\alpha_3 = 2.7$  and break energies  $\epsilon_{b,1} = 0.004$  eV and  $\epsilon_{b,2} = 0.6$  eV between  $2 \cdot 10^{-4}$  eV and 50 eV in the observer frame. The expected SSC emission is shown as the solid curve in the X-ray regime.

becoming dominant at radio wavelengths. A gradual steepening followed by a steep decline occurs above  $\sim 1$  eV caused by the cutoff in the electron distribution. Again synchrotron losses dominate the steady-state electron spectrum above the self absorption turnover energy. However, because the ratio  $u'_{\text{phot}}/u'_B$  is significantly higher than in Model H, the SSC component (solid curve at X-ray energies in Fig. 3) is potentially important in Model L.

Because pion photoproduction losses dominate over proton synchrotron losses for the present parameter set, the predicted  $\gamma$ -ray spectrum above 10 GeV is determined by synchrotron emission by charged pions and muons rather than by the protons themselves. Muon/pion synchrotron radiation naturally produces a high energy hump extending even up to TeV energies. Because pions and muons have a lower rest mass than protons, their synchrotron emission peaks at higher photon energies than the proton synchrotron radiation for the same Lorentz factor and magnetic field. While  $\mu^\pm/\pi^\pm$  synchrotron radiation dominates the energy output around the peak energy at  $\sim 100$  GeV, the emission in the EGRET energy range is due to proton synchrotron radiation, and extends down to soft  $\gamma$ -rays where the synchrotron radiation from the  $\pi$ -cascades takes over. Again, acceleration rate factor at the maximum proton energy  $\xi(E'_{p,\text{max}}) \approx 1$  is needed to explain photon emission up to TeV-energies.

Models with even lower jet-frame target photon densities could also be consistent with the data (except models with very low magnetic field values  $\leq 2$  G). However, the energy density stored in particles would be orders of magnitude below the magnetic energy density. If the size of the emission region were of order  $10^{14}$  cm or less, the resulting target photon density would reach values above  $10^{11.5}$  eV/cm $^3$ , and photopion production losses would cut off the injected proton spectrum at  $\sim 10^9$  GeV. In such models TeV-emission at a flux level as detected by HEGRA would be difficult to explain by proton or  $\mu^\pm/\pi^\pm$  synchrotron radiation.

## 5. Summary and discussion

We have made SPB model fits to the non-simultaneous SED of M87's nuclear emission, and find that all parameter sets which satisfactorily represent the data predict the main contribution to the high energy luminosity at about 100 GeV to be due to either  $\mu^\pm/\pi^\pm$  synchrotron or proton synchrotron radiation depending on whether the primary electron synchrotron component peaks at low (Model L) or high (Model H) energies, respectively.

In the EGRET energy range, the lower synchrotron peak energy model (Model L) predicts a softer spectrum than the fit with a higher synchrotron peak energy (Model H). While it is obvious that EGRET's sensitivity was more than an order of magnitude above the expected flux level from M87, we find that the satellite-based  $\gamma$ -ray instrument GLAST might possibly detect a weak signal from this radio galaxy (see Fig. 4).

In all the fits we have presented, the high energy radiation cuts off with a strong steepening in the TeV range in agreement with the spectral limits from the HEGRA observation. We also find that the HEGRA detection at  $>730$  GeV can only be explained if the proton acceleration rate is extremely high ( $\xi(E'_{p,\text{max}}) \approx 1$ ). We therefore expect M87, if it is indeed a mis-aligned SPB, could be an important source of UHECRs (see also Protheroe et al. (2003)).

For almost all proposed models of particle acceleration in different astrophysical environments,  $\xi(E)$  remains a rather uncertain model parameter. On the other hand, any postulation of acceleration of high energy protons in compact  $\gamma$ -ray production regions actually implies that  $\xi(E'_{p,\text{max}})$  at these energies should be close to unity, which corresponds to the maximum theoretically possible acceleration rate based on simple geometrical consideration (e.g.

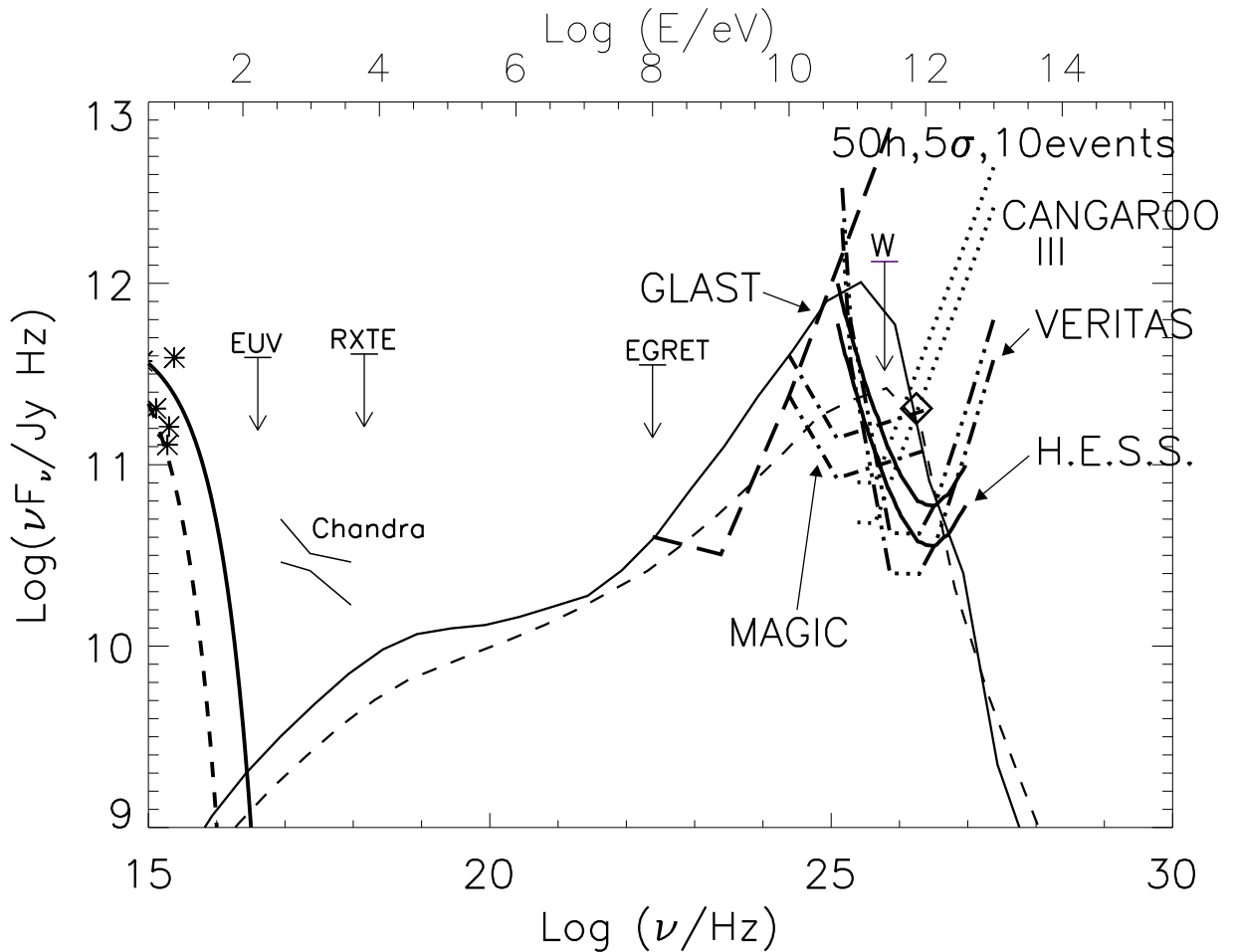


**Fig. 4.** Model H (solid line) and L (dashed line) fits compared with the sensitivities of  $\gamma$ -ray telescopes for a source at zenith and assuming a source photon spectrum  $\propto E^{-2.5}$  (thick lower lines) and  $\propto E^{-3.5}$  (thick upper lines); VERITAS: dashed-triple dotted lines; H.E.S.S. phase I: solid lines; MAGIC (from: "The MAGIC Telescope Project Technology and performance aspects": <http://hegra1.mppmu.mpg.de/MAGICWeb>): dashed-dotted lines; CANGAROO III (from: "Status Report of the CANGAROO-III Project": <http://icrhp9.icrr.u-tokyo.ac.jp/c-iii.html>): dotted lines. For the GLAST sensitivity (from: <http://glast.gfsc.nasa.gov/resources/brochures/gsd/>) a source photon spectrum  $\propto E^{-1.5}$  is used.

Hillas (1984)). An interesting possibility could be particle acceleration at the annihilation of magnetic fields in the fronts of poynting flux dominated jets (Blandford (1976); Lovelace (1976)). It has been argued that this mechanism could provide effective acceleration of extremely energetic protons with  $\xi(E'_{p,\max}) \sim 1$  (Haswell et al. 1992). A quantitative investigation of particle acceleration mechanisms is beyond the scope of this paper.

Both model fits presented seem to under-predict the emission in the radio domain as compared to the observations. Our modeling, however, assumes the same size for the emission region at all energies, while the data indicate a smaller width of the optical than the radio jet (Sparks et al. (1996)) though with *roughly* the same morphology. In addition, the inter-knot region is observed to be weaker in the optical than in the radio band (Sparks et al. (1996)). It appears therefore reasonable to attribute the missing flux in our model to the inter-knot region, and to a larger blob size in the radio band as compared to higher frequencies.

As previously noted, the Chandra data lie above the extrapolation of the optical spectrum to higher energies (Wilson & Yang (2002)). We point out that the modelled SED of M87 is based on non-simultaneous data, and that the X-ray flux could have been much lower than the Chandra data suggest at the time of the optical observations. Another critical point is that different resolutions of the images at the various energies have been used in the literature for the flux determinations. We have used for our compilation of the SED the highest resolution data available at each frequency, ranging from arcmin (HEGRA) to sub-arcsecond (Chandra, Hubble, VLBI) scales, and could introduce additional non-negligible uncertainties into the flux measurements. However, a flatter X-ray spectrum consistent with the Chandra data might be achieved if either the magnetic field is highly inhomogenous, or a secondary  $e^\pm$  population is responsible for the X-ray flux (Wilson & Yang (2002)).

While, in principle, the SPB model provides secondary synchrotron emitting  $e^\pm$ s from the various cascades which may extend even into the X-ray domain, the fits presented can not easily explain the high flux level observed at these energies as electron synchrotron radiation or as part of the high energy hump cascade component. Nevertheless, for magnetic fields of order a few Gauss SSC radiation might become detectable also in hadronic models. Fig. 3 shows that the SSC component peaks at X-ray energies with a spectral signature that is in agreement with the Chandra observations, but its flux is roughly an order of magnitude too low to explain the Chandra data. If the magnetic field or the size of the emission region were a factor  $\sim 3$  lower model L would predict the Chandra X-rays as SSC photons. The latter change moves model L slightly in the direction of model H. Thus, X-ray variability might be related to relatively small changes in the model parameters, raising or lowering the importance of inverse Compton losses with respect to synchrotron losses.

Another possible source for the observed emission in the Chandra band might be a contribution, either directly or reprocessed through cascading, from photon fields other than the primary electrons' synchrotron radiation. The spectral continuum data do not show any thermal bump from the putative accretion disk. Di Matteo et al. (2003) have shown that an advection dominated accretion disk could account for a large fraction of the observed X-ray nuclear flux. The radiative efficiency is extremely low, but the accretion rate is found to be large enough for Comptonization of the synchrotron emission of the disk or the thermal bremsstrahlung emission to dominate the X-ray emission (Di Matteo et al. (2003)). A sudden drop of one order of magnitude of the accretion rate could lower the X-ray disk output by  $\sim 2$  orders of magnitude.

For an advection dominated disk with a X-ray luminosity  $L_{\text{disk}} \approx 7 \times 10^{40}$  erg/s (Di Matteo et al. (2003)) the total energy density in the jet frame  $u'_{\text{disk}}$  can be derived through the transformation (see e.g. Dermer & Schlickeiser (2002))

$$u'_{\text{disk}} \approx 1.7 \cdot 10^{10} \text{ eV cm}^{-3} [\Gamma_j (1 - \beta_j \mu(r))]^2 \left( \frac{L_{\text{disk}}}{10^{40} \text{ erg s}^{-1}} \right) \left( \frac{r/\mu(r)}{10^{15} \text{ cm}} \right)^{-2}$$

where  $r$  is the distance of the jet plasma blob from the black hole,  $\mu(r) = r/(r^2 + r_{\text{in}}^2)^{1/2}$  and we have approximated the disk's radiation field as a luminous ring of radius  $r_{\text{in}}$  that illuminates the moving blob. Assuming a inner accretion disk radius of  $r_{\text{in}} = 1.23 r_g$  (for an extreme Kerr black hole of mass  $M = 10^9 M_\odot$ ) and taking  $\Gamma_j = 1.5$  one obtains  $u'_{\text{disk}} \sim 2 \cdot 10^{10} \text{ eV cm}^{-3}$  at  $r = 10^{15} \text{ cm}$  and  $\sim 2 \cdot 10^8 \text{ eV cm}^{-3}$  at  $r = 10^{16} \text{ cm}$ . Hence, for  $r \gtrsim 10^{16} \text{ cm}$  the accretion disk radiation proves to be unimportant as a target field for cascading and photon-particle interactions in M87 compared to the primary electron synchrotron emission.

Recently Donea & Protheroe (2003) have constrained the torus temperature of the torus to  $< 250$  K using existing data from the literature. On the other hand, during an extreme flaring state, related to the accretion rate changes or to a spin flip of the central black hole, the torus could undergo enough heating to become 'visible'. This alters the high energy part of the spectrum above several hundreds of GeV, as is discussed in Donea & Protheroe (2003). Therefore, a visibility-state of the torus (if present) could be achieved at the cost of not being able to observe very high energy gamma rays from the nucleus of M87. Regular monitoring of M87 at VHE gamma-rays and IR frequencies could be important to elucidate the problem of existence or non-existence of a dusty torus in M87. For a temperature of the torus radiation of  $< 250 \text{ K}$  the co-moving frame energy density is  $2 \cdot 10^7 \Gamma_j^2 \text{ eV cm}^{-3} \ll u'_{\text{phot}}$  for M87, and is therefore negligible as target photon field. The star and dust contribution of M87's host galaxy has been estimated to  $630 \Gamma_j^2 \text{ eV cm}^{-3}$  and  $6.3 \Gamma_j^2 \text{ eV cm}^{-3}$  in the jet frame, respectively (Stawarz et al. (2003)), and can obviously also be neglected regarding M87's synchrotron radiation density of order  $10^{10} \text{ eV cm}^{-3}$ .

Fig. 4 shows that the recently commissioned Cherenkov telescope array VERITAS, the southern arrays H.E.S.S. and CANGAROO III (though at large zenith angles  $> 45^\circ$ ), and MAGIC may be able to detect M87. The predicted integral fluxes  $> 100 \text{ GeV}$  for Models H and L are  $\sim 4 \times 10^{-11} \text{ cm}^{-2} \text{ s}^{-1}$  and  $\sim 4 \times 10^{-12} \text{ cm}^{-2} \text{ s}^{-1}$ , respectively. We have used A. Konopelko's simulator for the H.E.S.S. response (<http://pluto.mpi-hd.mpg.de/konopelk/WEB/simulator.html>) to estimate the necessary observation time for statistically significant detection. A 10 h on-source observation with the full phase I (four telescopes) H.E.S.S. array would result in a  $8 - 9\sigma$  detection (expected cosmic ray rate is  $\sim 0.7 \text{ s}^{-1}$ ,  $\gamma$ -ray rate is  $0.055 \text{ s}^{-1}$ ) in the case of a high-energy peaked photon target, and  $4 - 5\sigma$  detection in the case of the low-energy peaked photon target for 300 h of usable data assuming the source at zenith (expected cosmic ray rate is here  $\sim 0.7 \text{ s}^{-1}$ ,  $\gamma$ -ray rate is  $0.006 \text{ s}^{-1}$ ). Since the sensitivity of VERITAS (Weekes et al. (2002)) is similar to that of H.E.S.S., similar numbers can be expected for VERITAS observations. In Fig. 4 we summarize the minimum flux for a 50 h observation (with statistics exceeding 10 photons and a signal detection at a level of at least  $5\sigma$ ) using the phase I H.E.S.S. array, the VERITAS array, CANGAROO III and MAGIC (assuming the source at zenith) and GLAST, in comparison the the predicted high energy fluxes. Note, however, that these predictions are based on a non-simultaneous observed SED and, depending on the actual activity state of M87, the predicted fluxes and spectra may change significantly. In addition, absorption of  $\gamma$ -rays in infrared radiation from a putative torus could affect the spectrum above 1 TeV if the torus temperature  $T_{\text{torus}}$  were higher than 250 K, and above 200 GeV if  $T_{\text{torus}} \geq 1000 \text{ K}$  (Donea & Protheroe (2003)). Work is in progress to make SPB model fits to other nearby FR I radio galaxies.



In both models presented here, the power output in the high energy hump is roughly equal to the power output in the low energy hump of the SED. Because of M87's proximity, absorption of sub-GeV/TeV-photons in the cosmic infrared background radiation field is not expected to affect the spectrum below  $\sim 50$  TeV. *The observed spectral behaviour at high energies should be intrinsic to the source.* Tracing the spectrum at GeV-TeV-energies would give a  $\gamma$ -ray spectrum that for the first time includes an unabsorbed (by radiation fields external to the source) cutoff. These data could serve as a typical template BL Lac spectrum at source after correcting for M87's jet mis-alignment. By comparing this template with BL Lac spectra at high redshifts, meaningful constraints for the extragalactic background radiation field around IR wavelengths can be derived.

*Acknowledgements.* We thank A. Konopelko for providing us with his H.E.S.S. response simulator and fruitful discussions. AR's research is funded by DESY-HS, project 05CH1PCA/6, and that of RJP and ACD by an ARC Discovery Project grant.

## References

- Aharonian, F. and the HEGRA Collaboration 2003, A&A 403, L1  
 Ahn, E.-J., Medina-Tanco, G., Biermann, P.L., Stanev, T. 2000, astro-ph/9911123  
 Bai, J.M. & Lee, M.G. 2001, ApJ, 549, L173  
 Berghöfer, T.W., Bowyer, S., Korpela, E. 2000, ApJ, 535, 615  
 Biermann, P.L. & Strittmatter, P.A. 1987, ApJ, 322, 643  
 Biermann, P.L. 1997, J. Phys. G, 23, 1  
 Biermann, P.L., Ahn, E.-J., Kronberg, P.P., Medina-Tanco, G., Stanev, T. 2001, in Physics and Astrophysics of Ultra-High-Energy Cosmic Rays, vol. 576, ed. M. Lemoine & G. Sigl (Lecture Notes in Physics) 181  
 Billoir, P., Letessier-Selvon, A. 2000, astro-ph/0001427  
 Biretta, J.A., Sparks, W. B., Macchetto, F. 1999, ApJ, 520, 621  
 Biretta, J.A., Zhou, F., Owen, F.N. 1995, ApJ 447, 582  
 Biretta, J.A., Stern, C.P., Harris, D.E. 1991, AJ, 101, 1632  
 Blandford, R.D. 1976, MNRAS 176, 465  
 Blandford, R.D. & Znajek, R.L. 1977, MNRAS, 179, 433  
 Cohen, J.C. 2000, AJ, 119, 162  
 Curtis, H.D. 1918, Pub. Lick. Obs. 13, 31  
 Dermer, C.D. & Schlickeiser, R. 2002, ApJ, 575, 667  
 Di Matteo, T., Allen, S.W., Fabian, A.C., Wilson, A.S., Young, A.J. 2003, AJ, 582, 133  
 Donea, A.-C. & Protheroe, R.J. 2003, Prog. Theor. Phys. Suppl., 151, 186  
 Drury, L.O'C 1983, Rep. Prog. Phys., 46, 973  
 Falcke, H. & Biermann, P.L. 1995, A&A, 293, 665  
 "GLAST: Exploring nature's highest energy processes with the Gamma Ray Large Area Space Telescope" NASA document NP-2000-9-107-GSFC, February 2001, p29. <http://glast.gfsc.nasa.gov/resources/brochures/gsd/>  
 Götting, N. and the HEGRA Collaboration 2001, in Proc. 27th Int. Cosmic Ray. Conf., Hamburg, vol. 7, ed. M. Simon et al. (Copernicus Gesellschaft, Katlenburg-Lindau) 2669  
 Greisen, K. 1966, Phys. Rev. Lett., 16, 748  
 Hillas, A.M. 1984, ARA&A, 22, 425  
 Harris, D.E., Biretta, J.A., Junor, W., Perlman, E.S., Sparks, W.B., Wilson, A.S. 2003, ApJ, 586, L41  
 Haswell, C.A., Tajima, T., Sakai, J.J. 1992, ApJ, 401, 495  
 Junor, W., Biretta, J.A., Livio, M. 1999, Nature, 401, 891  
 Junor, W. & Biretta, J.A. 1995, AJ, 109, 500  
 Le Bohec, S. and the VERITAS Collaboration 2001, in Proc. 27th Int. Cosmic Ray. Conf., Hamburg, vol. 7, ed. M. Simon et al. (Copernicus Gesellschaft, Katlenburg-Lindau) 2643  
 Le Bohec, S. and the VERITAS Collaboration 2003, in Proc. 28th Int. Cosmic Ray. Conf., Tsukuba, Japan, vol. 5, ed. T. Kajita et al. (Universal Academic Press, Tokyo, Japan) 2627  
 Longair, M.S. 1994, High Energy Astrophysics Vol II, Cambridge University Press, Cambridge  
 Lovelace, R.V.E. 1976, Nature, 262, 649  
 "The MAGIC Telescope Project Technology and performance aspects": <http://hegra1.mppmu.mpg.de/MAGICWeb>  
 Marconi, A., Axon, D.J., Macchetto, F.D., Capetti, A., Soarks, W.B., Crane, P. 1997, MNRAS, 289, 21  
 Melrose, D.B. 1980, Plasma Astrophysics Vol I, Gordon & Breach, New York  
 Mori, M. 2000, in: "International Symposium on High Energy Gamma-Ray Astronomy", Heidelberg;  
 see also <http://icrhp9.icrr.u-tokyo.ac.jp/c-iii.html>  
 Mücke, A., Engel, R.R., Rachen, J.P., Protheroe, R.J. & Stanev, T. 2000, Comm.Phys.Comp., 124, 290  
 Mücke, A. & Protheroe, R.J. 2000, in Proc. workshop "GeV-TeV Astrophysics: Toward a Major Atmospheric Cherenkov Telescope VI", AIP Conf. Proc., Vol 515, ed. B.D. Dingus et al., 149  
 Mücke, A. & Protheroe, R.J. 2001, Astropart. Phys., 15, 121  
 Mücke, A., Protheroe, R.J., Engel, R., Rachen, J.P., Stanev, T. 2003, Astropart. Phys., 18, 593  
 Owen, F.N., Eilek, J.A., Kassim, N.E. 2000, AJ, 543, 611  
 Perlman, E.S., Sparks, W.B., Radoski, J., Packham, C., Fisher, R. S., Pina, R., Biretta, J. A. 2001, ApJ, 561, L51

- Protheroe, R.J., Donea, A.-C., Reimer, A. 2003 , *Astropart. Phys.*, 19, 559  
 Protheroe, R.J. & Clay, R.W. 2004, *Publications of the Astronomical Society of Australia*, Vol. 21, 1  
 Rachen, J.P. & Mészáros 1998, P., *Phys. Rev. D*, 58, 123005  
 Rachen, J. 2000, in *Proc. workshop "GeV-TeV Astrophysics: Toward a Major Atmospheric Cherenkov Telescope VI"*, AIP Conf. Proc., Vol 515, ed. B.D. Dingus et al., 41  
 Reimer, O., Pohl, M., Sreekumar, P., Mattox, J.R. 2003, *ApJ*, 588, 155  
 Reynolds, C.S., Fabian, A.C., Celotti, A. & Rees, M.J. 1996, *MNRAS*, 283, 873  
 Reynolds, C.S., Heinz, S., Fabian, A.C., Begelman, M.C. 1999, *ApJ*, 521, 99  
 Sparks, W. B., Biretta, J. A., Macchetto, F. 1996, *ApJ*, 473, 254  
 Stawarz, L., Sikora, M. & Ostrowski, M. 2003, *ApJ*, 597, 186  
 Urry, C.M. & Padovani, P. 1995, *PASP*, 107, 803  
 Weekes, T.C. and the VERITAS collaboration 2002, *Astropart. Phys.*, 17, 221  
 Wilson, A.S. & Yang, Y. 2002, *ApJ*, 568, 133  
 Zatsepin, G.T., Kuz'min, V.A. 1966, *JETP Lett.*, 4, 78

## Appendix A: Steady-state electron spectrum, maximum energies, synchrotron and SSC radiation

Consider a blob which is moving relativistically with Lorentz factor  $\Gamma_j$  and along the jet axis that is viewed from an observer at angle  $\theta$ . In the jet frame relativistic electrons are injected into the blob of size  $R'$  in the jet frame. We assume that pitch angle scattering maintains a quasi-isotropic particle distribution. Our interest is to derive the steady-state electron spectrum. In the following all quantities are in the co-moving frame of the jet, and we omit the primes for simplicity.

The number  $N(E)dE$  of particles with energy between  $E$  and  $E+dE$  in this region is governed by electron injection, synchrotron cooling process and particle escape on a time scale  $T_{\text{esc}}$ . It is described by the kinetic equation

$$\frac{\partial}{\partial E} \left[ \dot{E}N(E) \right] + \frac{N(E)}{T_{\text{esc}}} = Q(E) \quad (\text{A.1})$$

where

$$\dot{E} = -\frac{4}{3} \frac{\sigma_T c}{m_e^2 c^4} \left( \frac{B^2}{8\pi} \right) E^2 = -bE^2. \quad (\text{A.2})$$

with  $\sigma_T = 6.65 \cdot 10^{-25} \text{cm}^2$  the Thomson cross section. The first term in Eq. (A.1) describes the rate of energy loss due to synchrotron radiation averaged over pitch-angle (because of the isotropy of the distribution) in a magnetic field  $B$  (in Gauss), the second term particle escape from this region at an energy independent rate  $T_{\text{esc}}^{-1} = c/R'$ . Assuming an injection rate that follows a power law,  $Q(E) = Q_0 \cdot E^{-\alpha_e}$ , Eq. (A.1) has the solution

$$\begin{aligned} N(E) &= \frac{1}{|\dot{E}(E)|} \int_E^\infty dE' Q(E') \exp \left( -\frac{1}{T_{\text{esc}}} \int_{E'}^E \frac{dE''}{\dot{E}(E'')} \right) = \\ &= \frac{Q_0}{bE^2} \int_E^\infty dE' E'^{-\alpha_e} \exp \left[ \frac{1}{bT_{\text{esc}}} (E'^{-1} - E^{-1}) \right]. \end{aligned} \quad (\text{A.3})$$

For  $\alpha_e = 2$  and 3 the integral can be solved analytically, giving

$$N(E) = \frac{Q_0 T_{\text{esc}}}{E^2} \left[ 1 - \exp \left( \frac{E_c}{E_{\text{max}}} - \frac{E_c}{E} \right) \right] \quad (\text{A.4})$$

for  $\alpha_e = 2$ , and

$$N(E) = \frac{Q_0 b T_{\text{esc}}^2}{E^2} \left[ \frac{E_c}{E} - 1 - \exp \left( \frac{E_c}{E_{\text{max}}} - \frac{E_c}{E} \right) \left( \frac{E_c}{E} - 1 \right) \right] \quad (\text{A.5})$$

for  $\alpha_e = 3$ , with  $E_c^{-1} = bT_{\text{esc}}$  and  $E_{\text{max}}$  the maximum injected electron energy. In the case of injection powers  $\alpha_e \neq 2$  or  $\neq 3$  we solve the integral numerically.

The maximum energy,  $E_{\text{max}}$ , is limited by balancing energy gain and losses. The electrons may gain energy e.g. through particle acceleration. In general the acceleration time scale may be written as  $t_{\text{acc}} = E/[\xi(E)ecB]$  where  $\xi(E) \leq 1$  may be interpreted as an acceleration rate factor. A comparison with the observations yields typically very low values  $\xi(E_{e,\text{max}})$  at the maximum energy for electrons, while in the case of protons in hadronic models the rate factor is much higher at the maximum proton energy, typically  $\xi(E_{p,\text{max}}) = 10^{-3} \dots 1$ . The large difference between  $\xi(E_{p,\text{max}})$  and  $\xi(E_{e,\text{max}})$  can be naturally understood from the theory of plasma turbulence, since the electrons probe much smaller turbulence scales than the protons (Rachen (2000)). A more quantitative treatment of this issue has been presented by Biermann & Strittmatter (1987).

In acceleration theory the rate of energy gain is sensitively dependent on the upstream particle mean free path  $\lambda$ , which is given by

$$\lambda(E) = \frac{B^2 r_g}{8\pi I(k)k} \Big|_{k=1/r_g} \quad (\text{A.6})$$

in the small angle scattering approximation (Drury 1983) and with  $r_g$  the particle's gyro-radius. The magnetic turbulence spectrum  $I(k)$  is usually expressed as a power law of the wave number  $k$  in the turbulent magnetic field:  $I(k) \propto k^{-\beta}$ .  $\beta = 5/3$  corresponds to Kolmogorov turbulence, while  $\beta = 1$  corresponds to a fully-tangled magnetic field resulting in "Bohm diffusion", and is often considered for simplicity. For strong magnetic fields, Kraichnan turbulence  $\beta = 3/2$  may be present. The (parallel) diffusion coefficient is then given by  $\kappa_{\parallel} = \frac{1}{3}\lambda_{\parallel}v$  where  $v$  is the particle's speed and  $\lambda_{\parallel}$  is its mean free path parallel to the magnetic field. Hence,  $\kappa_{\parallel} \propto E^{\delta}$  where  $\delta = (2 - \beta)$ , and the acceleration time scale for the relativistic electrons and protons ( $r_g \propto E$ ) can then be expressed by  $t_{\text{acc}} \propto E^{\delta} \propto E/\xi(E)$ . In the following, we consider  $\delta$  to be a free parameter, and restrict our considerations to parallel shock fronts only for simplicity. Obviously,  $\xi_p(E) = \xi_e(E) = \xi(E) \propto E^{1-\delta}$  applies to both, electrons and protons. If the electron and proton spectra are limited by synchrotron losses, Biermann & Strittmatter (1987) found for their cutoff energy

$$\frac{\gamma_{e,\text{max}}}{\gamma_{p,\text{max}}} \propto (m_e/m_p)^{(3-\delta)/(1+\delta)}, \quad \frac{E_{e,\text{max}}}{E_{p,\text{max}}} \propto (m_e/m_p)^{4/(1+\delta)} \quad (\text{A.7})$$

and so one expects

$$\frac{\xi(E_{e,\text{max}})}{\xi(E_{p,\text{max}})} \propto (m_e/m_p)^{4(1-\delta)/(1+\delta)}. \quad (\text{A.8})$$

The ratio of their maximum synchrotron photon energies can readily be computed to:

$$\frac{\epsilon_{\text{syn},e}}{\epsilon_{\text{syn},p}} = \left( \frac{m_e}{m_p} \right)^{(5-3\delta)/(1+\delta)}. \quad (\text{A.9})$$

The acceleration model parameters used to calculate the SEDs of M87 can be understood for  $\delta \sim 0.3$  which is close to that for a Kolmogorov turbulence spectrum.

To obtain the synchrotron specific luminosity, for the case of no synchrotron self-absorption, as a function of frequency  $\nu$  we convolve the particle density  $N(E)$  with the synchrotron Green's function  $P(\nu, E)$ :

$$L_0(\nu) = \int dE P(\nu, E) N(E) \quad (\text{A.10})$$

with

$$P(\nu, E) = \frac{\sqrt{2}}{2\pi c} e^2 \omega_e F\left(\frac{\nu}{\nu_c}\right). \quad (\text{A.11})$$

for relativistic particles of velocity  $\approx c$  and an isotropically distributed magnetic field.  $\omega_e = eB/m_e$  is the electron gyro frequency and  $\nu_c = \sqrt{\frac{3}{2}}\omega_e E^2/(m_e^2 c^5)$  the critical frequency after pitch angle averaging. The function  $F(x)$  with  $x = \nu/\nu_c$  can be approximated by (Melrose 1980)

$$F(x) = x \int_x^{\infty} dx' K_{5/3}(x') \approx 1.85x^{1/3} \exp(-x). \quad (\text{A.12})$$

Synchrotron self-absorption will dominate the photon spectrum at low energies. The synchrotron radiation and its corresponding electron spectrum may be approximated by a multiple broken power law. For each part of the particle spectrum that is governed by a simple power law with index  $\alpha_{e,i}$  one can therefore use the absorption coefficient for synchrotron radiation of a power law electron distribution in a randomly oriented magnetic field (Longair 1994), which reads

$$\chi_{\nu,\text{ssa}} = \frac{\sqrt{2}e^3}{8\pi m_e} \left( \frac{\sqrt{6}\omega_e}{2\pi m_e^2 c^5} \right)^{\alpha_e/2} q_0 B \Gamma\left(\frac{3\alpha_{e,i}+2}{12}\right) \Gamma\left(\frac{3\alpha_{e,i}+22}{12}\right) \nu^{-(\alpha_{e,i}+4)/2} \quad (\text{A.13})$$

where  $q_0$  is  $Q_0$  divided by the source volume. The synchrotron specific luminosity in the jet frame is then

$$L(\nu) = \frac{L_0(\nu)}{\tau_{\nu,\text{ssa}}} [1 - \exp(-\tau_{\nu,\text{ssa}})]. \quad (\text{A.14})$$

with  $\tau_{\nu, \text{ssa}} = R \chi_{\nu, \text{ssa}}$ . Note, that for high magnetic fields that are typical for the SPB-model, the electron spectrum, and thus its corresponding synchrotron spectrum above the synchrotron-self absorption break energy, is often completely determined by synchrotron losses for typical blazar 'blob' sizes.

This synchrotron component represents the target photon field for photopion production and cascading in the SPB-model, and simultaneously manifests itself as the 'synchrotron hump' in the blazar SED after transformation of the luminosity  $L(\nu)$  into the observer frame. To save CPU-time we fit this target photon field with a multiple broken power law, which is then used as an input into the SPB Monte-Carlo code (see Sect. 3).

The importance of Inverse Compton scattering off the synchrotron photons produced by the same primary electron component is determined by the ratio of the synchrotron photon energy density and the magnetic field energy density. For  $B > 0.6(u_{\text{phot}}/10^{10}\text{eV cm}^{-3})^{1/2}$  Gauss the target photon density  $u'_{\text{phot}}$  is smaller than the magnetic field energy density, which is typically true for hadronic SPB models, and inverse Compton losses of the primary electron population can usually be neglected. In the following we calculate the expected SSC (jet frame) specific luminosity from an electron spectrum Eq. (A.3) in the Thomson limit which is valid for  $E \ll (m_e c^2)^2 / h\nu$ . In the  $\delta$ -function approximation it is given by:

$$L_{SSC}(E_\gamma) = c\sigma_T E_\gamma \int_0^\infty d\epsilon n(\epsilon) \int_{\gamma_{e,\min}}^{(m_e c^2)/\epsilon} dE N(E) \delta(E_\gamma - \gamma_e^2 \epsilon) . \quad (\text{A.15})$$

where  $\gamma_{e,\min} m_e c^2$  is the minimum injected electron energy and  $n(\epsilon)$  is the (jet frame) synchrotron photon density. For the calculations in Fig. 1 and 3 we performed the  $\epsilon$ -integration numerically.